AD-A074 746 ATOMIC WEAPONS RESEARCH ESTABLISHMENT ALDERMASTON (EN--ETC F/G 20/5
THE CONSTRUCTION AND PERFORMANCE OF TEAL,(U)
JUN 79 P L EGGINS, R J PROSSER, A C SIMMONS

UNCLASSIFIED AWRE-O-9/79 DRIC-BR-69056 NL

| OF |
AD
A074746

END
DATE
FILMED
11-79
DDC

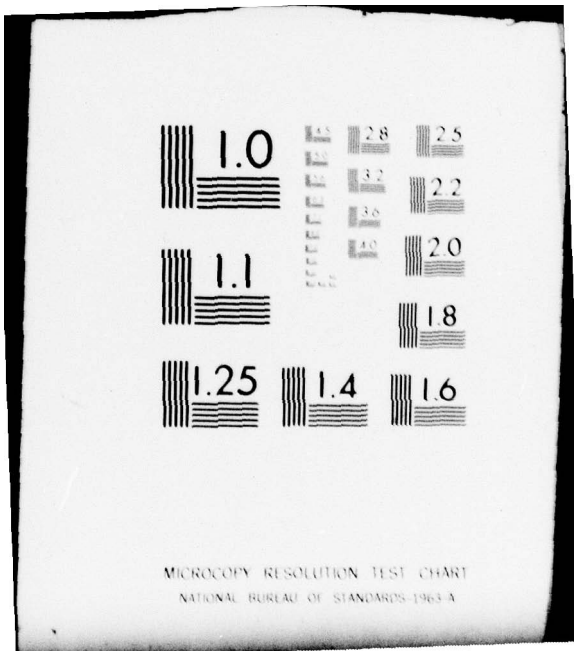
1.0
1.1
1.25
1.4
1.6
2.8
3.2
3.6
4.0
2.5
2.2
2.0
1.8
MICROCOPY RESOLUTION TEST CHART
NATIONAL BUREAU OF STANDARDS-1963-A

AWRE REPORT No. O 9/79

The Construction and Performance of TEAL

P L Eggins
R J Prosser
A C Simmons

UNLIMITED

Procurement Executive - Ministry of Defence

AWRE, Aldermaston

AWRE REPORT NO. 09/79

(12) 34

(6) The Construction and Performance of TEAL

(10) P L Eggins
R J Prosser
A C Simmons

(14) AWRE-O-9/79

(11) Jun 79

Recommended for issue by

E M Gunnersen, Superintendent

Approved by

J W Weale, Senior Superintendent

(18) DRIC

(19) BR-69056

046 650

JOB

ISBN O 85518129 X

CONTENTS

SUMMARY

The construction of TEAL (Transversely Excited Atmospheric pressure Laser) is described with reference to the required specification for single pulse thermal blooming experiments. All the major performance parameters are described, such as energy, temporal profile, spectrum and stability. In particular, several different measurements of the spatial profile are compared with theoretical predictions, which in general predict well the main features but not the finer details. Also the results of pulse stretching experiments are described, in which the pulse is lengthened from 3 to 14 μs.

1. INTRODUCTION

A CO_2 laser with certain properties was required for single pulse thermal blooming experiments. In order to compare experiment with theory it was essential that the properties of the laser beam were well characterised, reproducible from shot to shot, and conformed to the following requirements:-

(1) A pulse energy of at least 1 J.

(2) An axisymmetric spatial profile, which, when focussed, gave a near diffraction limited shape. This was required in order to facilitate theoretical modelling using an axisymmetric (3D) computer code. Also the spatial profile had to be independent of time during the pulse for the same reason.

(3) Shot to shot directional stability very much better than ± 54 μrad, this being the angle subtended by the smallest detector used. This should be maintained over at least 10 successive shots.

(4) A reproducible temporal profile.

(5) A reproducible spectrum, consisting preferably of only one or two rotational lines in the 10.6 μm band.

The laser used was a double discharge TEA laser with a continuously flowing gas mixture of $He:N_2:CO_2$ in the ratio 6:1:1, and with an unstable confocal optical resonator. The laser is referred to as TEAL.

2. LASER DESIGN

2.1 Electrical design

The charging circuit, shown in figure 1, is similar to that described by Pan et al. (1). The uniformity of the main anode/cathode discharge depends on the presence of a relatively uniform "layer" of electrons produced in the initial discharge between the trigger wires and the cathode.

In the original design, the trigger wires ran lengthways along the cathode plate and this resulted in a laser near field pattern, see figure 2, with a transverse modulation associated with the spacing of the trigger wires. Clearly, the initial electron distribution was not entirely uniform. Subsequently, a new cathode was substituted with transverse trigger wires, which eliminated this problem.

Laser action commences ≃ 3.6 μs after the initiation of the discharge and lasts for ≃ 3 μs. When C_1 is charged to 50 kV (≃ 300 J) the optical output is typically 10 J giving an overall efficiency of 3.3%.

2.2 Optical design

An unstable confocal optical cavity was chosen because it has certain well known (2) useful properties when a high power single mode output is required from a high gain gas laser.

A schematic of the resonator is shown in figure 3. Both mirrors are made of BeCu, which has a reflectivity of 98% at 10.6 μm. The convex output mirror is supported by a three-legged "spider" which inevitably interrupts the annular output. This arrangement was found to be preferable to mounting the mirror on an output window for several reasons:-

(1) It facilitates checking or replacement of the mirror or window independently.

(2) It allows the output window to be set at a large angle to the optical axis in order to eliminate back reflections which might disturb the mode structure or temporal profile.

(3) It provides a rigid mirror mount, easily centred.

The effect of the "spider" on the far field pattern is shown in figure 4. The ring modulation, in multiples of three, is clear but the central spot does not show any three-fold structure on this burn pattern, nor on any other burn patterns.

Alignment of the optical cavity is accomplished by allowing the beam from an HeNe laser to enter through a $\frac{1}{2}$ mm diameter hole in the centre of the concave mirror. The area of this hole is < 0.02% of the mirror area, so its effect on the laser output should be negligible. A glass flat prevents gas leaking through the hole. The HeNe laser beam in the cavity spreads initially by diffraction, and then as a result of the unstable cavity geometry, to form a visible annular output very similar to the pattern produced by the CO_2 laser beam, and having the same alignment requirements. Alignment of the cavity by successive mirror adjustments is then straightforward.

2.3 Mechanical design

In order to meet the requirements for shot to shot stability of beam direction and spatial profile, a massive and rigid mechanical design was required. The main reason for this was the transient rise in gas pressure, generated each time the laser is fired, which caused the mirrors to lose their alignment. The problem could have been avoided by mounting the mirrors external to the KCl windows. However, this would have required windows of higher optical quality, because they would be an integral part of the optical cavity, and, in addition, would have increased the optical losses, over and above the 75% output coupling. The method adopted was to use mirror mounts sufficiently robust to maintain mirror alignment against disturbances. Figure 5 shows the design.

The mirror mounting backplates are of 1 in. thick mild steel and are rigidly connected together by four 1½ in. diameter steel bars. This structure is mounted on a ½ ton steel table, and provides a very stable structure on to which the mirrors can be mounted. The perspex box which retains the gases, and into which the electrodes are mounted, is connected to the backplates by flexible bellows. These allow for differential thermal expansion of the perspex relative to the steel bars and also for coarse adjustment of the mirror spacing.

The mirrors are mounted kinematically with two powerful springs adjacent to each mounting point. The force exerted by these six springs is sufficient to overcome the transient gas expansion. Concentric with each mirror mount is a flexible rubber gas seal which allows adjustment of the mirror and also serves as a pressure relief valve, as close as possible to the mirror. Any relative movement between the mirror mount and its mounting plate is monitored by permanently fixed micrometer dial gauges. The mounts were found to be sufficiently robust that when deliberately displaced and allowed to reset by the action of the springs, any change in angular alignment of the mirror was too small to measure (< 5 μrad).

The mirror separation has coarse adjustment by moving one of the mounting plates along the steel bars before clamping it. Fine adjustment is provided by making one of the ball and socket pivots in the kinematic mounts adjustable with a screw thread by ± 5 mm.

3. LASER BEAM PROPERTIES

3.1 Energy

Total energy was measured using a Gen-Tec ED500 pyroelectric joulemeter. This was placed so as to receive the energy diffracted into the second order of a calibrated wire transmission grating. The energy was found to be typically ~ 10 J with a shot to shot variation of ~ ± 5%. It was also found that during a rapid succession of shots, the energy decreased with time due to the loss of CO_2 molecules by dissociation in the discharge.

3.2 Temporal profile

The temporal profile was measured using a photon drag detector, see figure 6. The profile is typical of a pulsed CO_2 TEA laser. There is an initial gain switched spike, containing ~ 25% of the total energy and lasting for ~ 200 ns, the remainder of the energy being emitted over a period of 3 μs.

The fast response time of the detector (< 1 ns) reveals the self-mode locking, which is another characteristic of CO_2 TEA lasers.

3.3 Laser spectrum

The laser spectrum is important because the absorption coefficient of propane, which is used in thermal blooming experiments, is sensitive to wavelength.

The spectrum of the laser output, as a function of time, was measured using an infra-red grating spectrum analyser (Optical Engineering Model 16A). Observations of the phosphor screen shown most energy to be in the P(20) rotational line of the 10.6 μm band, with a small amount in the P(18) and occasionally P(16) lines. Time resolved relative intensity measurements were made by replacing the phosphor screen with an array of Cr/CrO thin film detectors (3) with elements aligned with the positions of these lines. Numerous measurements showed a mean energy distribution:-

P(20)	82 ± 17%
P(18)	14 ± 12%
P(16)	4 ± 8%

The temporal profiles of these three lines showed no significant differences in shape.

To determine if any lines other than P(20), P(18) and P(16) of the 10.6 μm band were present at too low an energy to be observed on the phosphor screen, measurements were made of the energy transmitted through a calibrated narrow band pass optical filter, with a bandwidth of 0.25 μm, a band centre at 10.6 μm and a peak transmission of 78%. Outside the range of experimental error, ~ ± 15%, no energy was observed in other lines. The accuracy of this measurement was limited by the fact that the filter transmission varies very rapidly in the region of interest. Taking into account the possibility of up to 15% of energy in lines other than P(20), P(18) and P(16), the measured energy distribution becomes:-

P(20)	76 ± 22%
P(18)	13 ± 12%
P(16)	3.5 ± 7.5%
Other	7.5 ± 7.5%

3.4 Shot to shot stability

In order to monitor the spatial and temporal profiles of successive laser pulses in a reproducible way, it was essential that the position of the beam relative to the detector array did not vary from shot to shot. The criterion used was that over 10 successive shots the scatter of the beam centre position in the measurement plane should be much less than the dimensions of a single element of the detector array, ie, much less than 0.8 mm. The measurement plane was the focal plane of a two mirror optical system with an effective focal length of 14.8 m, so that an angular scatter < ± 54 μrads was required. The effects of air turbulence on the beam stability were minimised by enclosing most of the beam patch in 4 in. diameter plastic tubing.

Measurements of the position of the beam centre were made by observing the burn marks produced by successive shots on heat sensitive paper, using an alignment telescope with cross wires. These measurements showed typically an rms scatter of ± 0.2 mm (± 14 μrads) which is well within the requirement.

3.5 Refractive index of the laser medium

The accuracy with which the spatial profile of the laser beam fits the simple diffraction theory depends partly on the accuracy with which the optical cavity has been constructed, but also on the homogeneity of the refractive index in the laser medium, ie, in the gas discharge. The variation of refractive index in space and time was investigated using a Mach-Zehnder interferometer with an HeNe laser, see figure 7. The interference pattern contains information relating to the refractive index difference between the probe and reference arms of the interferometer, integrated along the length of the laser medium, parallel to its optical axis. The HeNe laser beam probes a region of cross section 1 cm^2 on each shot. The interference pattern was photographed every 1 μs during the discharge using an IMACON high speed camera. By repeating this procedure in different regions of the discharge on successive shots, refractive index contour maps were produced for different times during the discharge, see figure 8. A constant refractive index gradient across the laser would result in an angular displacement of the beam, whereas a variable gradient would be expected to cause distortion of the beam profile.

3.6 Spatial profile

Using these refractive index data, theoretical predictions were made of the spatial profile in the far field (4). This was accomplished by computing the effect on an initially plane wave of a typical refractive index profile, as the wave propagates through the laser medium. The refractive index profile corresponding to 1 μs from the start of the laser pulse of ~ 3 μs duration was used. By taking an average, static profile, rather than attempting to account for the time variation of refractive index changes, the computation was considerably simplified and because the temporal variation of refractive index is not large, this should give a good indication of the beam distortion induced by laser medium inhomogeneities. The effect was computed of multiple passes of a beam through the laser medium, the computation being continued until a steady state situation resulted. This was taken as a prediction of the phase and intensity distribution across the near field of the laser output. By a Fourier transform the far field distribution was then predicted. A calculation of the pattern was also performed assuming a uniform refractive index throughout the laser medium. Also, the far field pattern was calculated for a plane wave diffracted by an annular aperture of the same dimensions as the laser output annulus (5).

In order to test these theoretical profiles, the spatial profile of the focussed beam was measured in two different ways. Firstly, using an eight element linear array of Cr/CrO thin film detectors, each element 0.8 × 1 mm. A profile was built up from several laser shots. Results obtained in this way are shown in figure 9 in comparison with a theoretical profile (4) assuming a uniform refractive index throughout the laser medium. These measurements were made in the plane of a × 4 magnified image of the primary focus, in order to ease the problem of making measurements on a very small scale.

One of the fundamental criteria of beam quality is the Strehl ratio β (6), which is the ratio of the on axis intensity in the focal plane diffraction pattern, to the theoretical diffraction limited on axis intensity for a uniform plane wave. For an ideal beam $\beta = 1$, and any aberration of the beam will decrease the value of β. It can be seen from figure 9 that the Strehl ratio is close to unity, implying a high quality beam.

Secondly, the focal plane profile was measured by observing the energy within a known radius, as a function of radius, ie, the integrated energy distribution. These measurements were carried out by placing a variable circular aperture of known radius on the beam axis in the focal plane, and in front of a pyroelectric joulemeter. Energy normalisation of each shot was made by placing a calibrated diffraction grating in the main laser beam and monitoring with another joulemeter the total energy transmitted into the second order of diffraction. Figure 10 shows the experimental results, together with several theoretical predictions. Firstly, a profile generated as described above (4), taking into account the measured refractive index gradient across the laser medium. Secondly, the prediction of another computer code (7) which starts with a near field profile and calculates the profile in the nominal focal plane without assuming that it is a true far field profile. Thirdly, the result of the plane wave diffraction theory for an annular aperture of appropriate dimensions.

The theoretical model which takes into account the refractive index inhomogeneities within the cavity (4) is the one which most accurately predicts the measured fraction of energy within the central maximum, but none of the theories predict the wide spread of energy outside the central maximum.

In order to examine in more detail the properties of the beam when focussed by a good quality mirror which introduces negligible spherical aberration or astigmatism, several further experiments were carried out.

Firstly, the thin film array was used to measure the profile of the central maximum at 10 cm intervals along the axis of the focussing beam from 350 to 390 cm, straddling the nominal focus at 370 cm from the mirror, see figure 11. The measurements were made in the × 4 magnified image of the focal region. It can be seen that the on axis intensity increases beyond 370 cm, also the spot diameter decreases with increasing distance through the nominal focus and does not show any symmetry about the focus.

Secondly, the axial position of peak intensity was determined. This was done by firing the laser at sufficiently high intensity to generate air breakdown in the focal region. Although the positions of dust particles, which are necessary for the initiation of air breakdown, are random, the mean position of air breakdown over a series of shots occurs at the position of peak intensity. Over a series of 10 shots this was found to be at 384 ± 6 cm from the focussing mirror, ie, 14 cm beyond the nominal focus at 370 cm.

Thirdly, a series of burn patterns were made on exposed polaroid film at 10 cm intervals along the beam. From these, the diameter of the first dark ring was measured as a function of axial position. This was found to decrease linearly through the focal region. It was also noticed that, in the nominal focal plane, the fourth bright ring of the diffraction pattern was clearly more intense than the third, see figure 4.

In order to determine whether these features are to be expected of an idealised annular laser beam, these results were compared with theoretical predictions. Taking the last result first, the idealised plane wave theory of diffraction by an annular aperture with the same dimensions as the laser output (5) predicts, in the far field, a profile in which the fourth bright ring is more intense than the third, which is in agreement with the experimental result. However, the theory also predicts that the fifth bright ring should be more intense than the fourth, which is not observed experimentally. This may be attributable to the fact that the laser output is not an ideal plane wave.

In order to make theoretical predictions of the profile at positions other than the focal plane, a computer code using an implicit finite-difference method to solve the wave equation (7) was used to predict the beam profile at any axial position for any given axisymmetric near field intensity and phase profile. It could not, therefore, take into account the three-legged mirror support, nor the effect of refractive index distortion within the laser medium. The calculation was carried out with four near field profiles, see figure 12.

The first case, 01, is the ideal case of constant phase and intensity across the annulus. The second, 02, has constant phase with an intensity profile derived from the computer model (4) of the laser. The third, 03, also has constant phase but with an intensity profile derived from experimental measurements, which are different from the computer predictions. Finally, the phase predictions of the computer model are added to the experimental intensity profile for case 04.

Figure 13 shows the intensity on axis in the region of the focus, together with experimental measurements of on axis intensity and the position of peak intensity as determined from the air breakdown measurements. The fit of curves 01 and 03 is good up to and including the position of peak intensity, but the solitary experimental point beyond the peak is not accurately predicted by any of the theoretical models.

Figure 14 shows the radius of the first dark ring of the diffaction pattern, compared with experimental results. This is seen to decrease approximately linearly through the focal region, the best fits in this case being curves 02 and 04.

Figure 15 shows the fraction of the total energy contained within the central maximum as a function of distance along the direction of propagation. The measured fraction at 370 cm is also shown. None of the curves is a good fit, 02 being the best.

Clearly, none of the four models gives a good fit for every property. In particular 04, which most closely resembles the laser output, is not significantly a better fit than any of the others. Two possible reasons for these discrepancies are firstly, the beam asymmetries which cannot be modelled with the present codes, or secondly, it may be that the fine structure of the near field pattern has some significant effect on the beam profile in the focal region. This fine structure is visible in figure 16 which is a burn pattern showing the near field intensity and shows numerous narrow concentric rings, associated with which there may be oscillations in phase. This fine structure cannot be predicted by the computer models because their scale is finer than the mesh size used in the computations. Nevertheless, all four models predict a complex beam profile with continously decreasing central spot radius through the focal region and different positions for the peak intensity and maximum fraction of energy in the central spot, which means that these large-scale features cannot be attributed to any imperfections in the beam.

Finally, using the thin film array, measurements were made of the temporal variation of the spatial profile. Figure 17 is typical of a large number of measurements of this type which show that there are small changes in the shape of the profile with time, apart from changes in magnitude. The thin film

array was aligned vertically, because the refractive index measurements indicated that any gross movement of the beam would be in the vertical plane. From the refractive index measurements shown in figure 8, an estimate was made of the expected beam movement, using the paraxial ray equation

$$\frac{1}{n}\frac{dn}{dx} = \frac{d\phi}{dz},$$

where dn/dx is the transverse refractive index gradient, and $d\phi/dz$ is the rate of bending with distance along the laser axis. Between 1 and 2 μs the calculated movement was in the range 0.01 to 0.1 mm, upwards. Such movements would be at the limit of resolution of the detector array. However, careful analysis of numerous profiles indicated that the beam did move in the expected direction and that its movement was consistent with the theoretical prediction. The movement amounted to 1 to 10% of the central spot diameter at the focus and the velocity of the movement was 10 to 100 m/s.

4. PULSE STRETCHING WITH CO

There was a requirement for a laser pulse of significantly longer duration than the 3 μs of the laser in its original form. Now it has been shown (8) that, by the substitution of CO for N_2 in the laser medium and by a change in the volume ratios of the constituent gases CO_2:CO:He, an increase in excess of 100 μs in the pulse length is possible. By trial and error it was found that a gas flow ratio CO_2:CO:He of 0.4:0.6:8 litres/min produced the maximum pulse length of 14 μs with an energy of 4 J. Figure 18 shows that the temporal profile consisted of a leading spike 0.5 μs long with 14% of the total energy and a relatively low intensity tail extending to 14 μs.

The reason for the relatively small increase in pulse length may be related to the output coupling and consequent ratio of CO_2:CO required to maintain laser action. The laser pulse is sustained in the presence of CO because, in addition to storing energy in the first vibrational excited state, as N_2 does, and then slowly transferring it to the CO_2 upper laser level by inelastic collisions, the presence of CO also leads to more efficient depopulation of the lower laser level, which N_2 does not. This means that a population inversion can be maintained with a relatively small upper laser level population. When an unstable resonator is used, with inherently higher output coupling than a stable resonator, coherent radiation must be generated at a correspondingly rapid rate in order to overcome the output coupling losses. Thus, the reservoir of energy in the vibrationally excited CO molecules is more rapidly depleted and laser action is terminated. In order to extract this energy at a sufficiently rapid rate, a relatively large number of CO_2 molecules is required. Thus, when using a high output coupling resonator a high CO_2:CO ratio is necessary.

This hypothesis is supported by the following experimental evidence. Using a stable resonator (8) an increase in the output coupling from 2% to 5% resulted in a decrease in pulse length from 120 to 90 μs. The present unstable resonator has an output coupling of 75% and a maximum pulse length of 14 μs. The optimum CO_2:CO ratio in the low output stable resonator was 1:20 and for the high output unstable resonator was 1:1.2. Thus, it may be possible to control the pulse length by means of the output coupling coefficient and adjusting the CO_2:CO ratio for maximum energy.

4.1 Long pulse spectrum

The spectrum was investigated in exactly the same way as with the CO_2:N_2:He gas mixture. It was found that ≃ 97% of the energy was in the P(20) rotational component of the 10.6 μm band and the remainder in the P(18) component. There was no evidence of energy in any other component or band.

4.2 Long pulse spatial profile

The spatial profile in the far field, as a function of time, was measured using the eight element thin film array. A typical set of profiles is shown in figure 19. It is clear that the beam profile changes significantly during the 14 μs of the pulse. The direction of movement of the beam centroid was found, over many shots, to be always the same. This was the direction expected from the measurements of refractive index changes in the CO_2:N_2:He laser medium. There is no reason to think that the sign of the refractive index gradient will be different in the CO_2:CO:He mixture, although a realistic comparison of measured and calculated movement would require a knowledge of the refractive index contours in the CO_2:CO:He mixture during the 14 μs of the pulse. This movement is a severe limitation to the usefulness of the long pulse for single pulse thermal blooming experiments and consequently no further refractive index measurements were made. It may be a fundamental limitation of the double discharge method of excitation, because the refractive index changes result from the energy deposition profile in the laser medium, and this profile is characteristic of the double discharge system.

5. CONCLUSIONS

A thorough investigation of the TEAL output has shown it to be suitable for use in thermal blooming experiments, although certain characteristics are undesirable. To summarise:-

(1) The laser output energy was ≃ 10 J, which greatly exceeds the minimum requirement of 1 J.

(2) The temporal profile, although complex, is constant from shot to shot and can be dealt with by thermal blooming theory. However, because of the rapid changes in intensity during the gain switched spike, any thermal blooming measurements in the first 200 ns will be difficult to make with any reliability.

(3) The laser spectrum consists of at least three rotational lines in the 10.6 μm band, of which the predominant one is P(20). Subsequent measurements of the absorption coefficient of propane showed a variation of ± 20% which is attributed mainly to shot to shot variations in the laser spectrum. This can be accommodated in thermal booming theory by making calculations assuming highest and lowest probable absorption coefficients.

(4) The shot to shot beam movement of ± 14 μrad was well within the requirements of less than ± 54 μrad for accurate profile measurements.

(5) Refractive index measurements within the laser can account for deviations of the central maximum of the spatial profile from the ideal, and for the small movements of the beam during each pulse, neither of which should invalidate thermal blooming measurements.

(6) The pulse length can be increased from 3 to 14 μs by replacing nitrogen with carbon monoxide in the laser gas mixture. However, because of the large changes which occur in the spatial profile during each pulse, it is unsuitable for thermal blooming experiments. Nevertheless the ability to change the pulse length by more than a factor of 4 will make the laser more versatile in experiments where the highest stability is not required.

6. ACKNOWLEDGMENTS

Our thanks are due to Messrs W A Waller and D J Hay for implementing the mechanical design of the laser.

REFERENCES

1. Yu-Li Pan, A F Bernhardt and J R Simpson: Rev Sci Instr, 43, 662-666 (1972)

2. A E Siegman: Laser Focus, 42-47 (May 1971)

3. N A MacLean and L E Collins: J Phys D, 11, 999-1007 (1978)

4. A T Jones, Rolls Royce: Private Communication (1977)

5. H Lamberton, SERL: Private Communication

6. M Born and E Wolf: "Principles of Optics". Pergamon (1970)

7. P D Roberts, AWRE: Private Communication

8. D C Hamilton: Optics Comm, 19, 339-342 (1976)

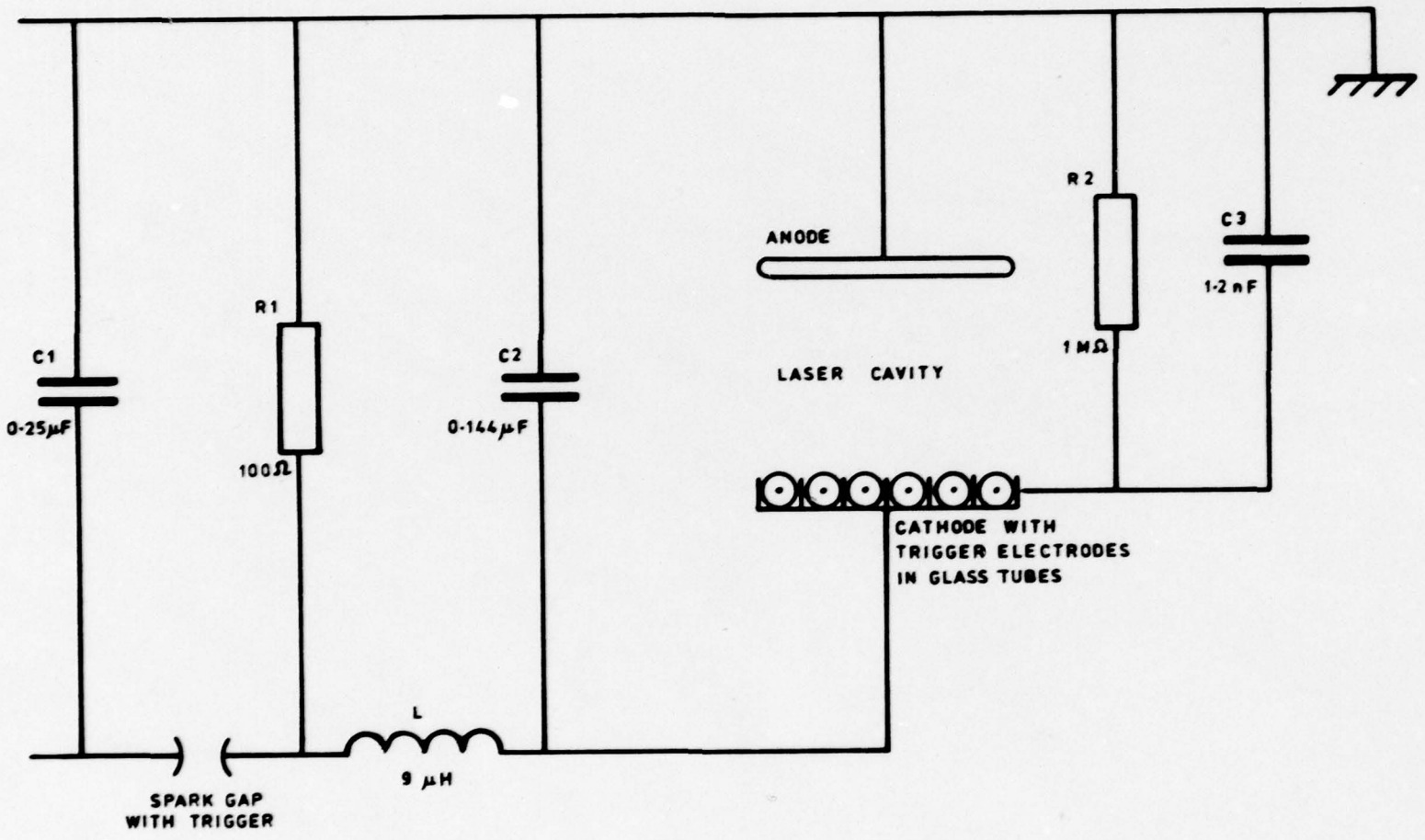

FIGURE 1. Electrical Design of TEAL

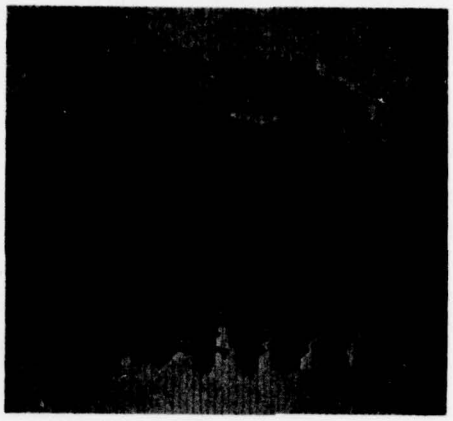

FIGURE 2. NEAR FIELD BURN PATTERN SHOWING STRIATIONS CAUSED BY THE USE OF LONGITUDINAL TRIGGER ELECTRODES. THE OPTICAL CAVITY CONSISTED OF PLANE PARALLEL MIRRORS, ONE OF WHICH WAS PARTIALLY TRANSMITTING

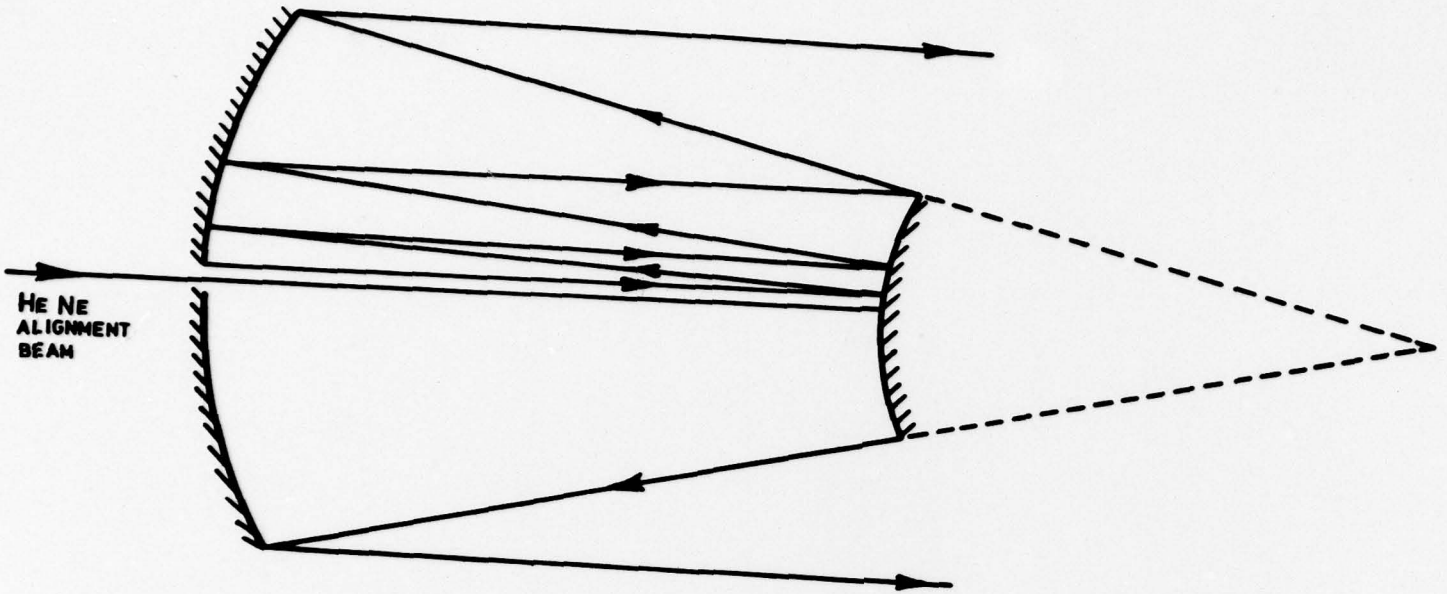

RADIUS OF CURVATURE	$R_1 = 643$ cm
	$R_2 = -310$ cm
MIRROR DIAMETER	$d_1 = 3.94$ cm
	$d_2 = 1.81$ cm
MIRROR SEPARATION	$L = 166.5$ cm
MAGNIFICATION	$M = R_1/R_2 = 2.07$
FRESNEL NUMBER	$N_f = 20.02$
EQUIVALENT FRESNEL NO	$N = N_f\frac{(M-1)}{2M^2} = 2.5$

FIGURE 3. Optical Design of TEAL

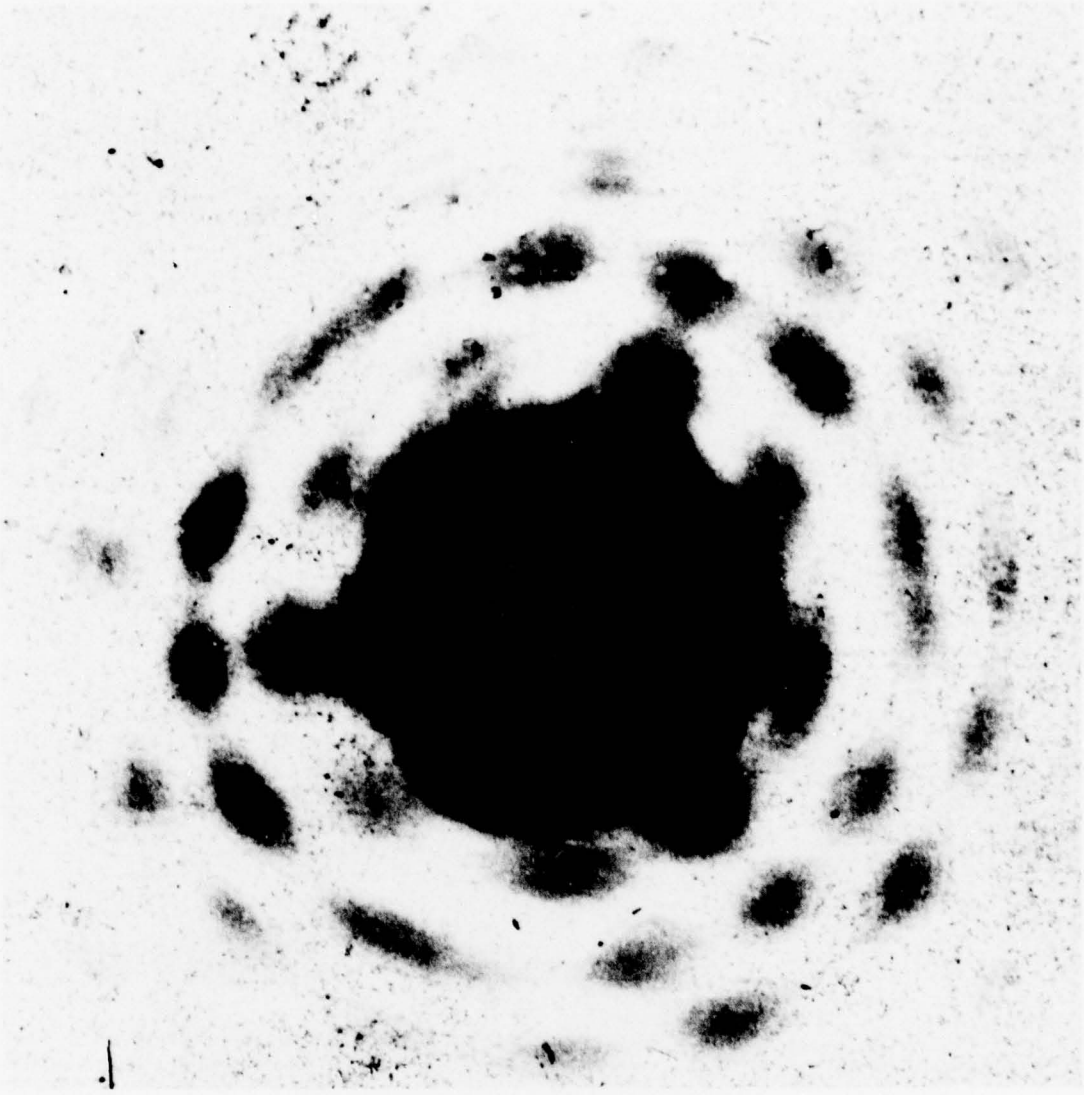

FIGURE 4. FAR FIELD BURN PATTERN SHOWING THE RING MODULATION

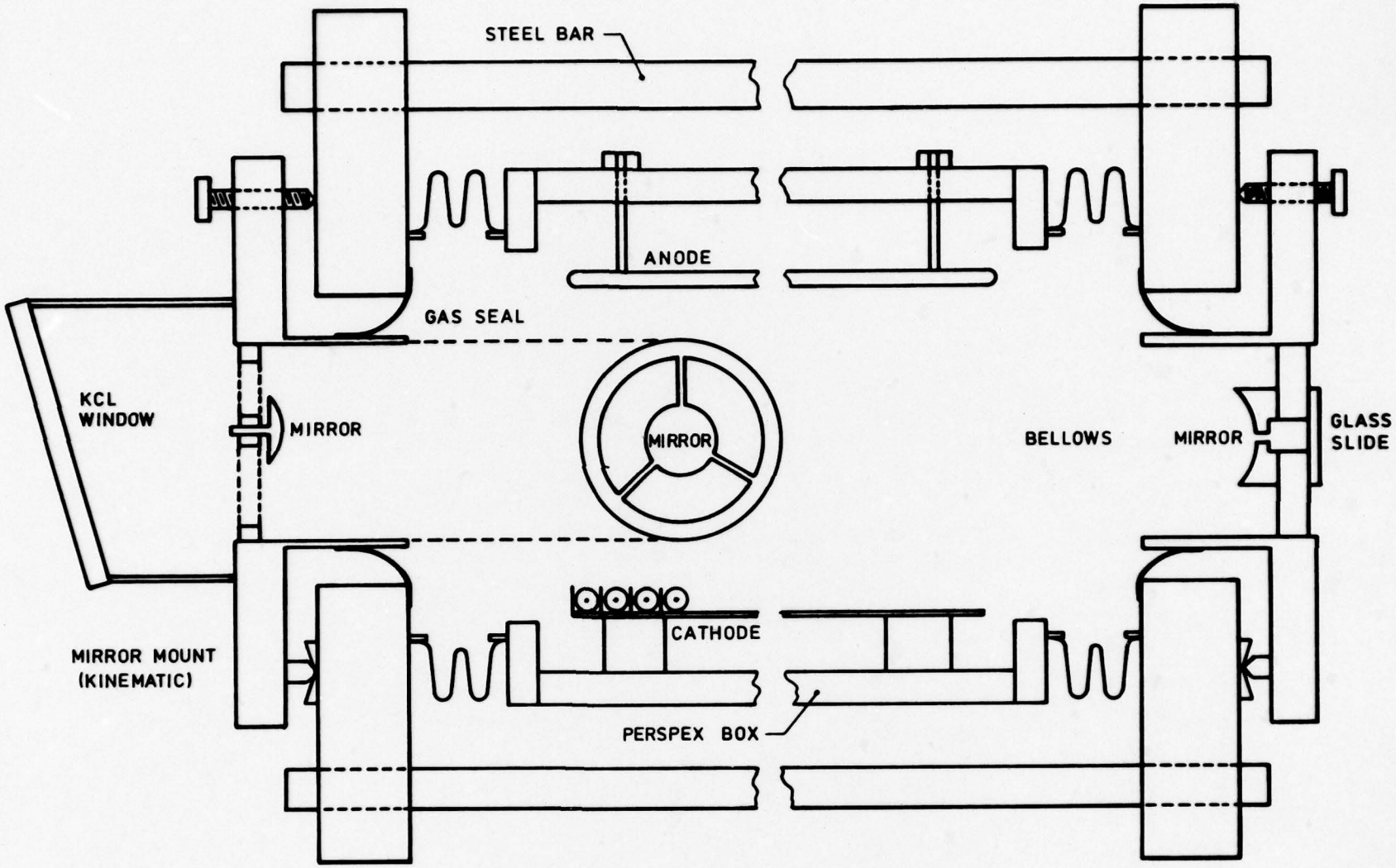

FIGURE 5. Mechanical Design of TEAL

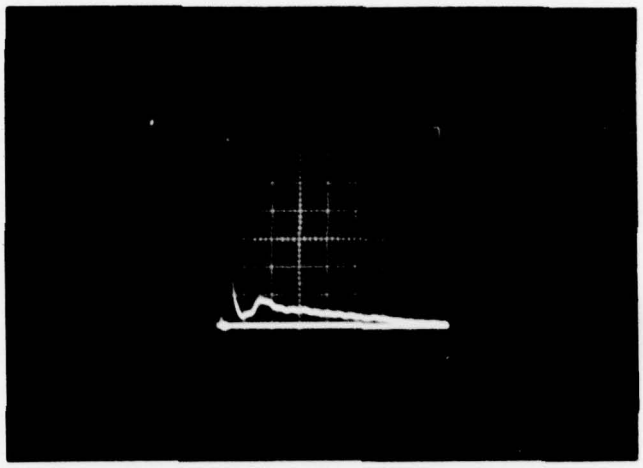

0.2 μs per division
(Limited bandwidth oscilloscope)

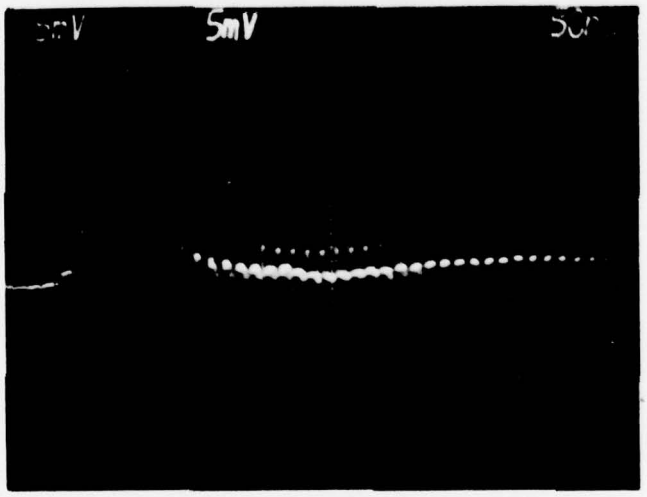

0.05 μs per division

FIGURE 6. TEMPORAL PROFILE OF TEAL

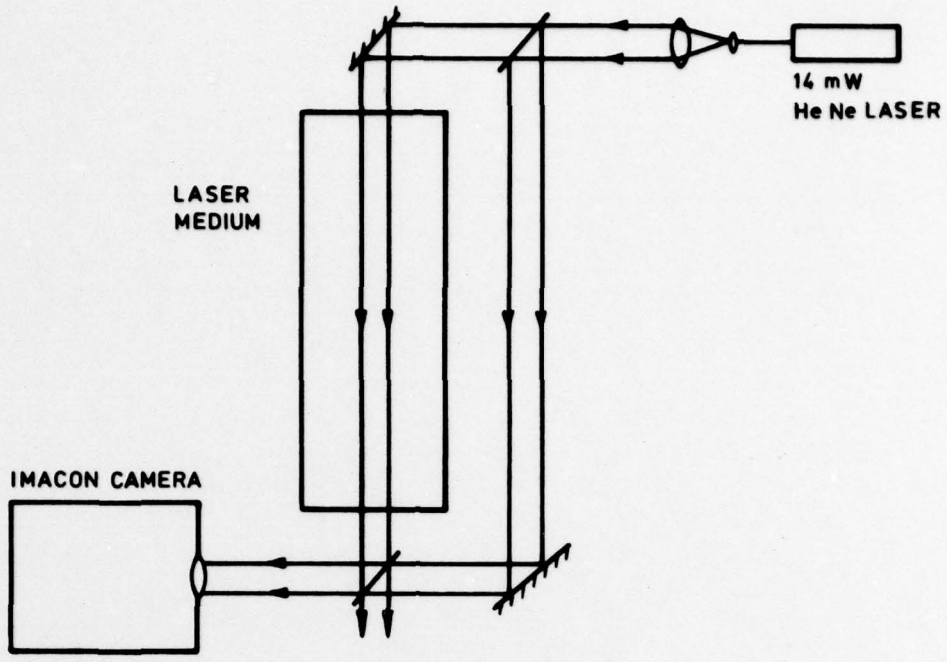

PLAN OF MACH-ZEHNDER INTERFEROMETER

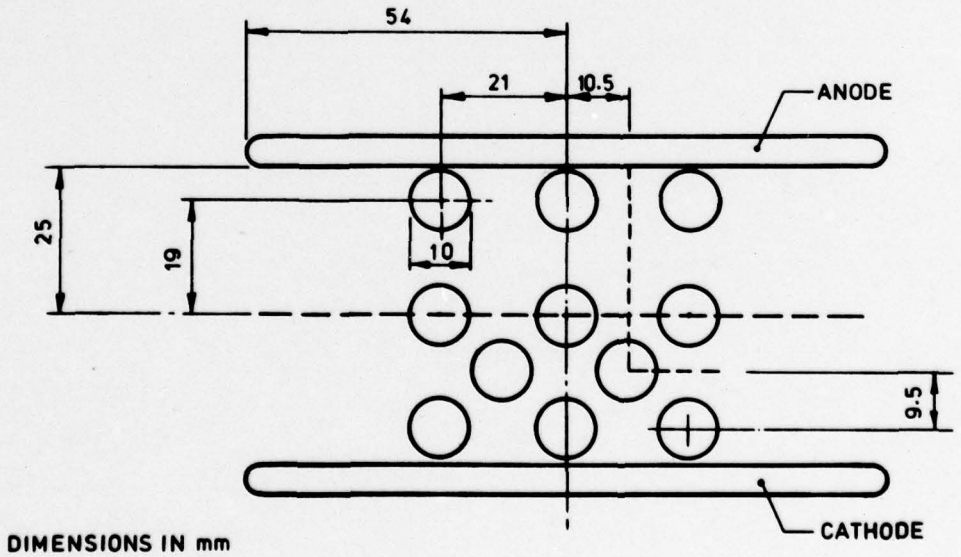

DIMENSIONS IN mm

FIGURE 7. Section through the Laser Medium showing the Positions of the Probe Beam

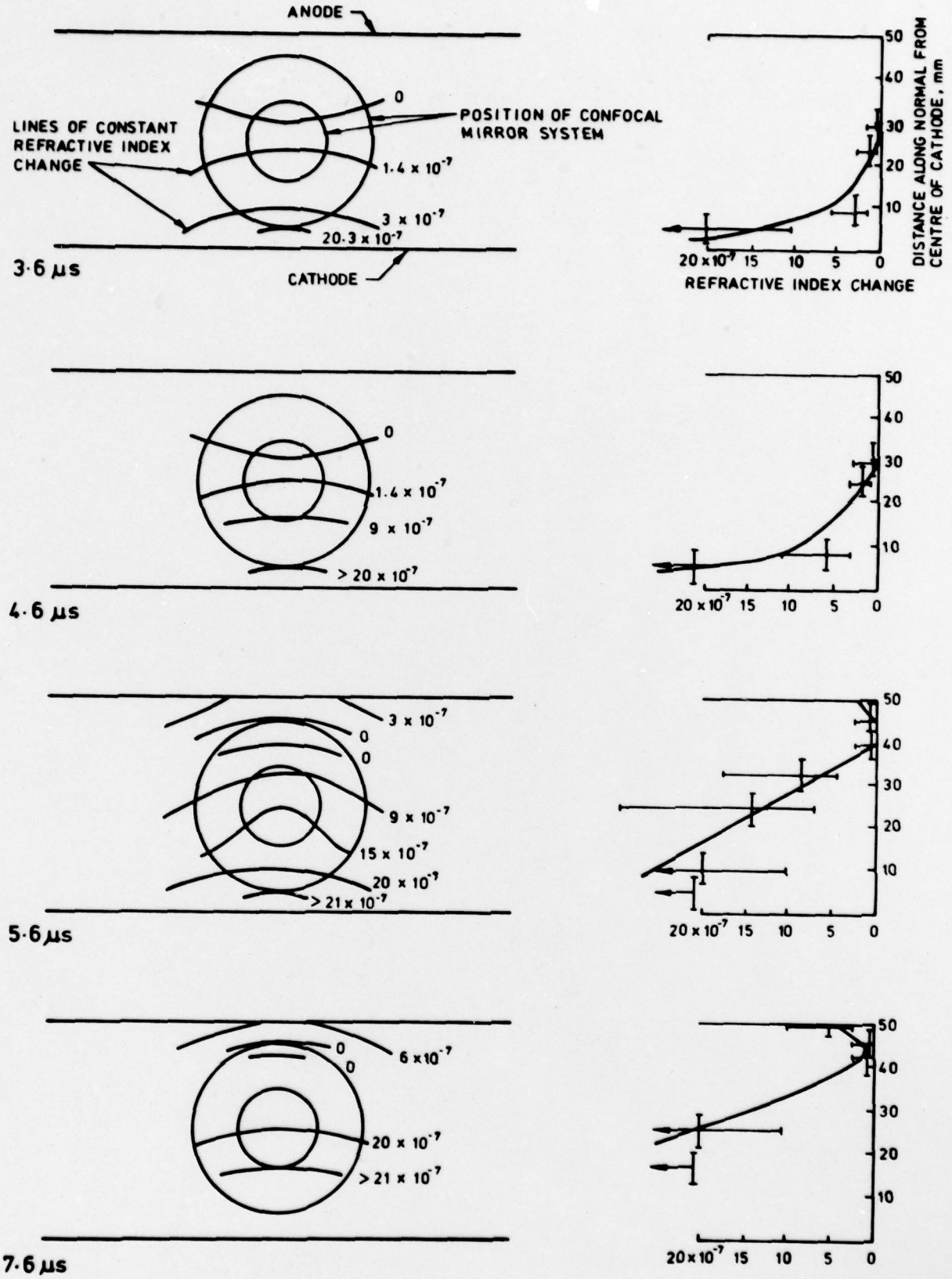

FIGURE 8. Refractive Index Contours as a Function of Time. Charging Voltage 50kV. Laser Action commences 3·6μs after the start of the Voltage Pulse

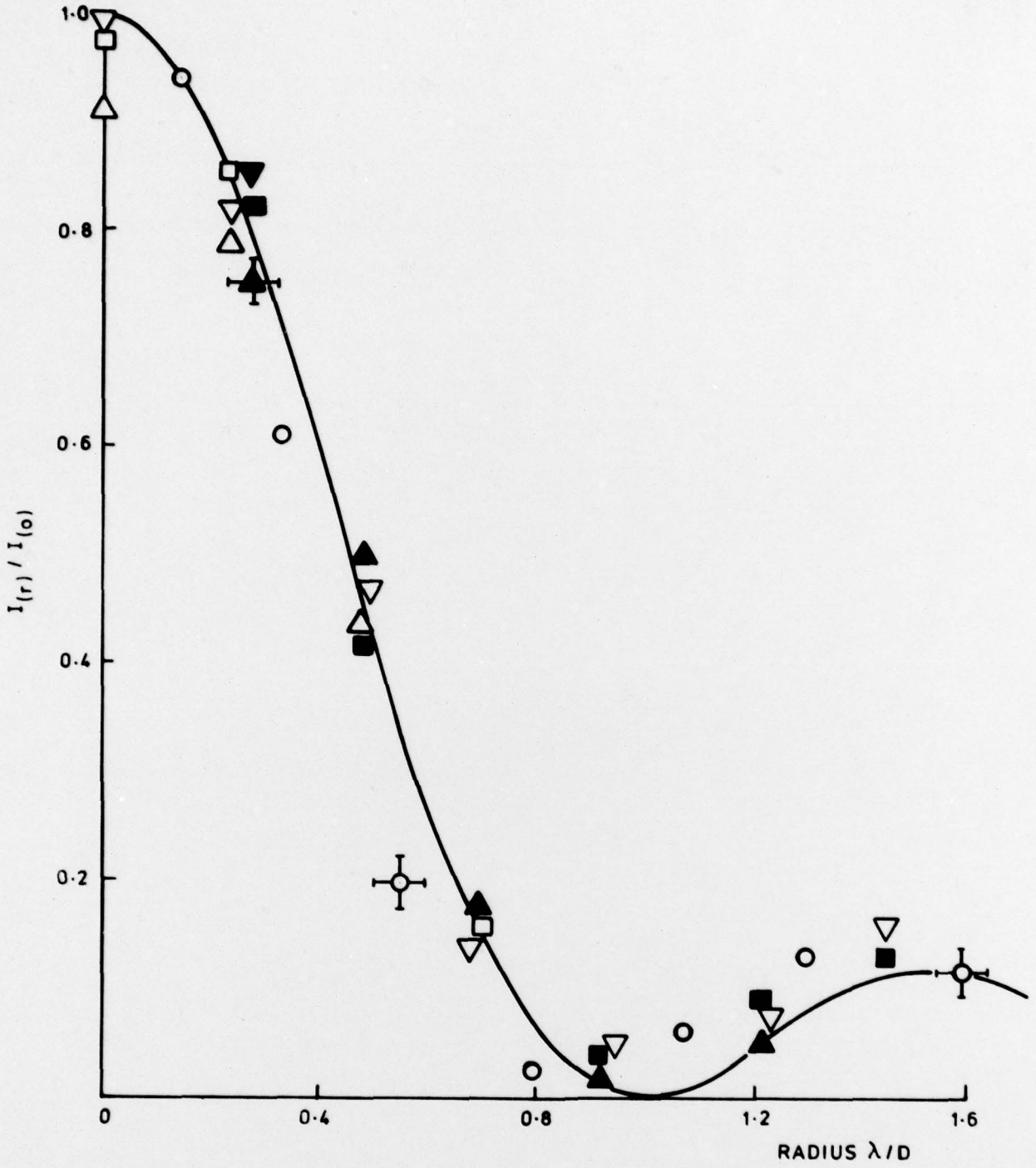

FIGURE 9. Theoretical Model of TEAL Focused Profile (4) and Experimental Measurements

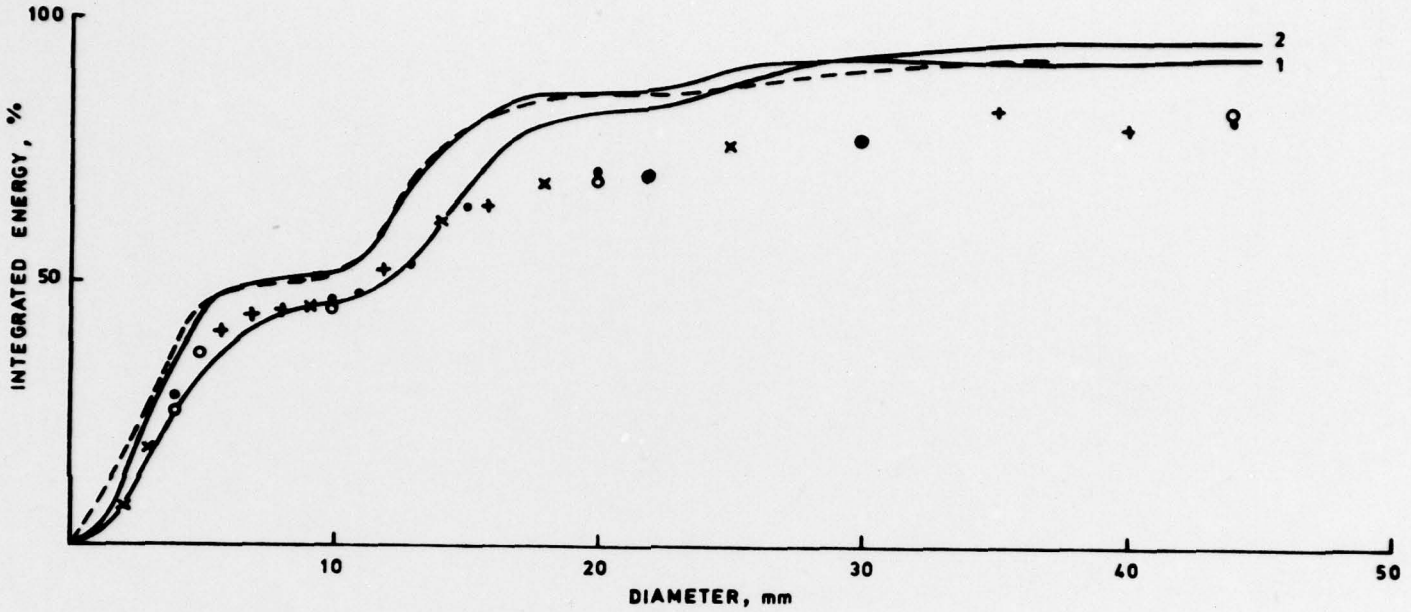

EXPERIMENTAL RESULTS FROM FOUR RUNS - x + o •

THEORETICAL PROFILES - 1 PLANE WAVE THEORY (5)

2 COMPUTER MODEL OF LASER MEDIUM (4) WITH REFRACTIVE INDEX GRADIENT INCLUDED

- - - - - COMPUTER MODEL (7)

FIGURE 10. Focal Spot Integrated Energy

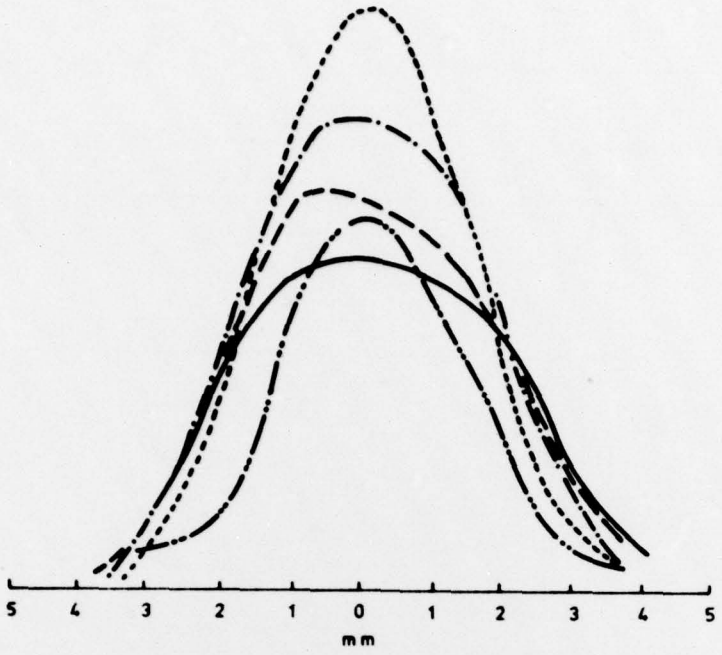

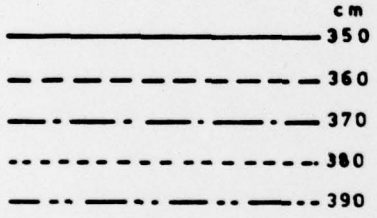

NUMBERS REFER TO AXIAL DISTANCES FROM FOCUSSING MIRROR. ALL PROFILES ARE TAKEN 1 μs FROM THE START OF THE PROFILE

FIGURE 11 Measured Relative Intensity Profiles of the Beam Central Maximum at 10 cm Intervals between 350 cm and 390 cm

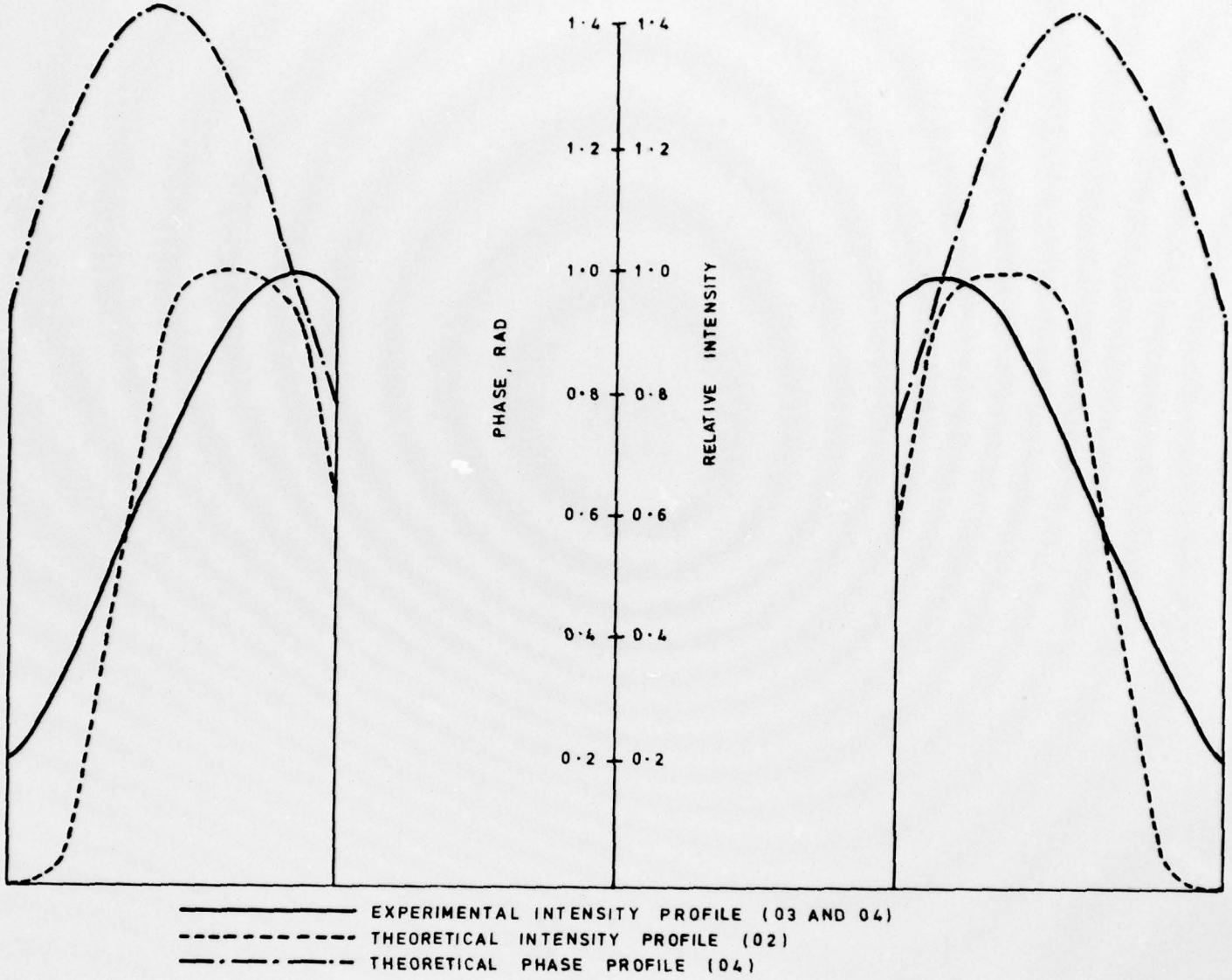

FIGURE 12 Near Field Profiles used in Propagation Calculations

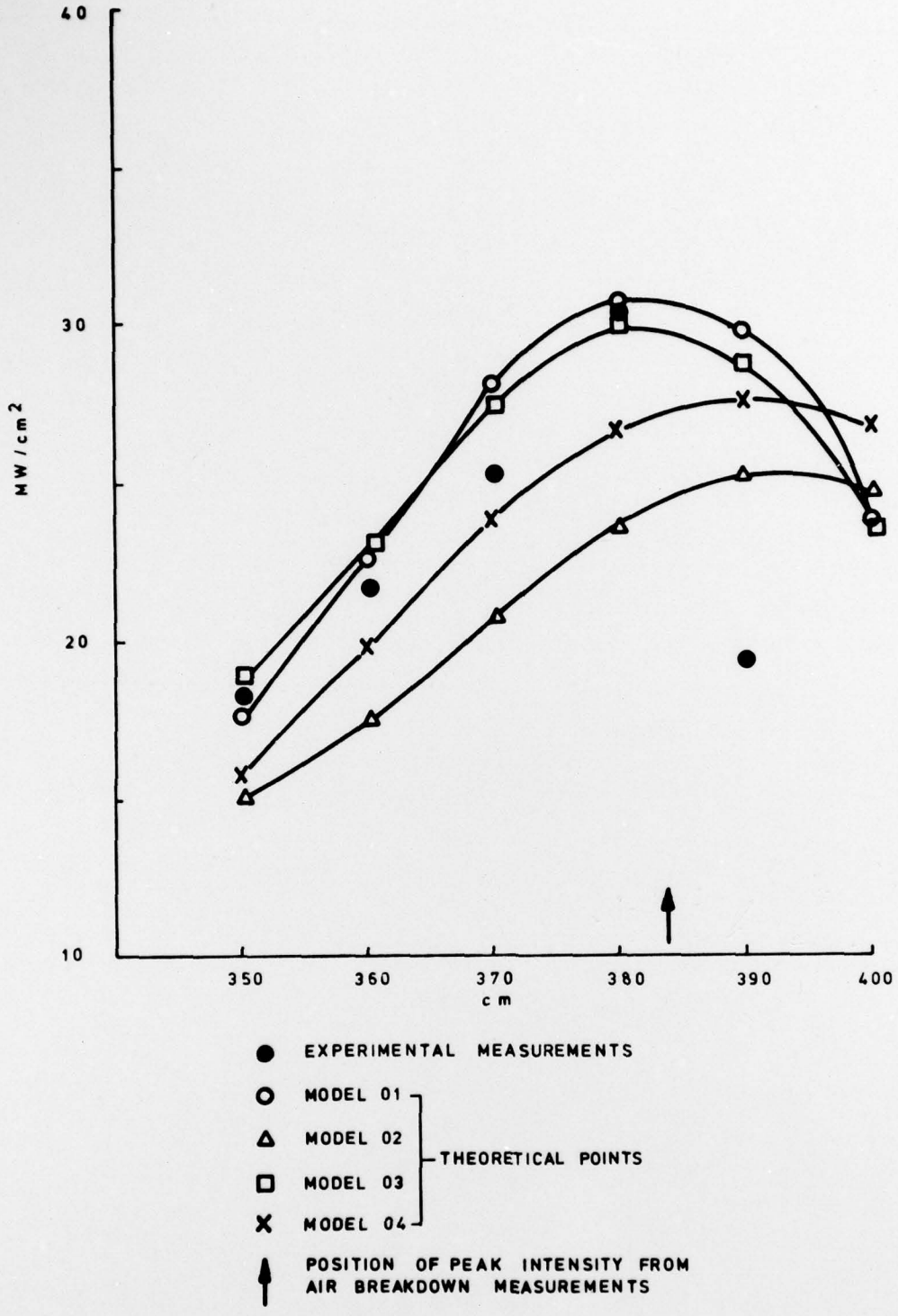

FIGURE 13 On Axis Intensity versus Distance from Mirror with 370cm Focal Length

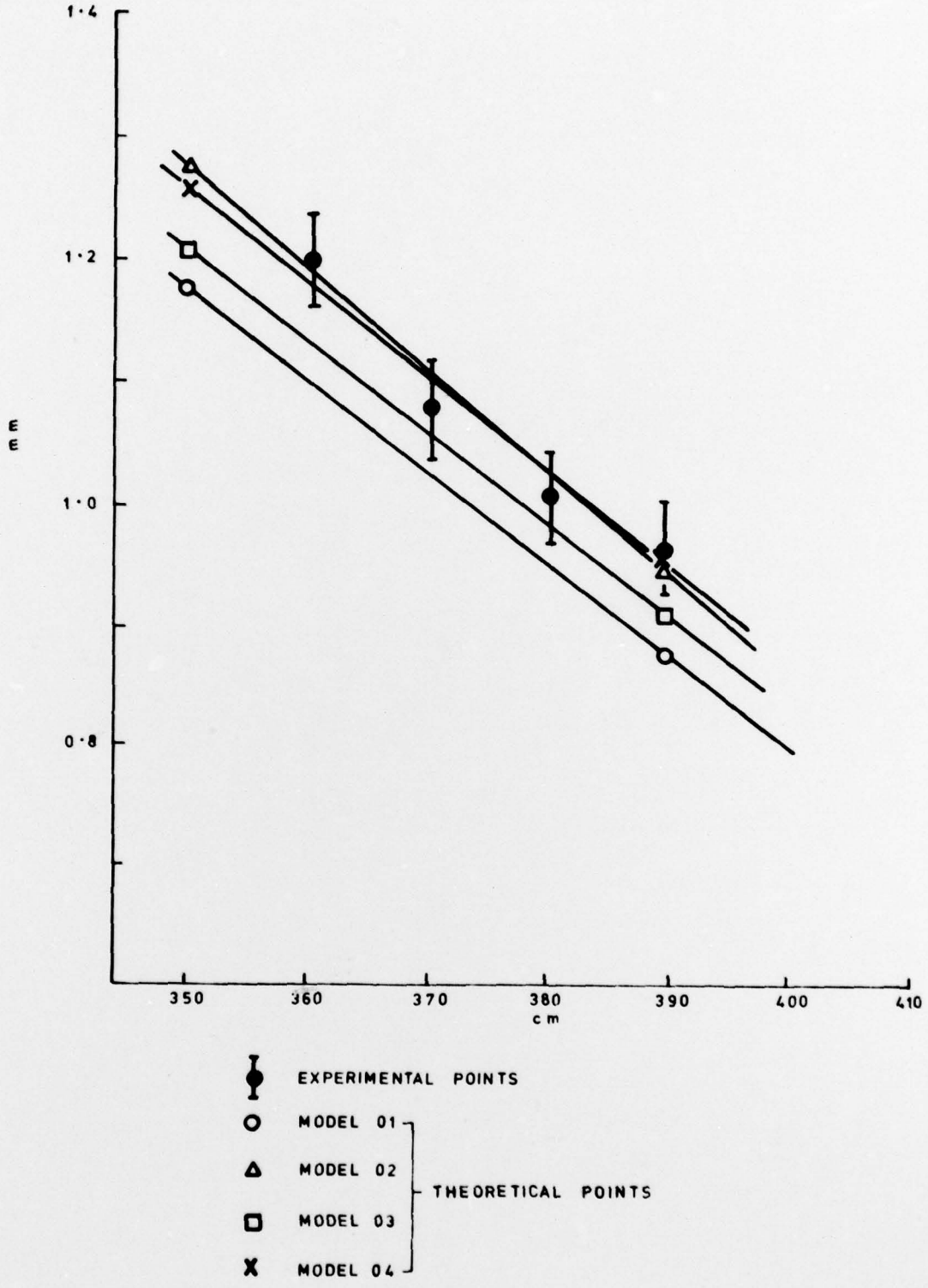

FIGURE 14 Radius of the First Dark Ring versus Distance from 370cm Focal Length Mirror

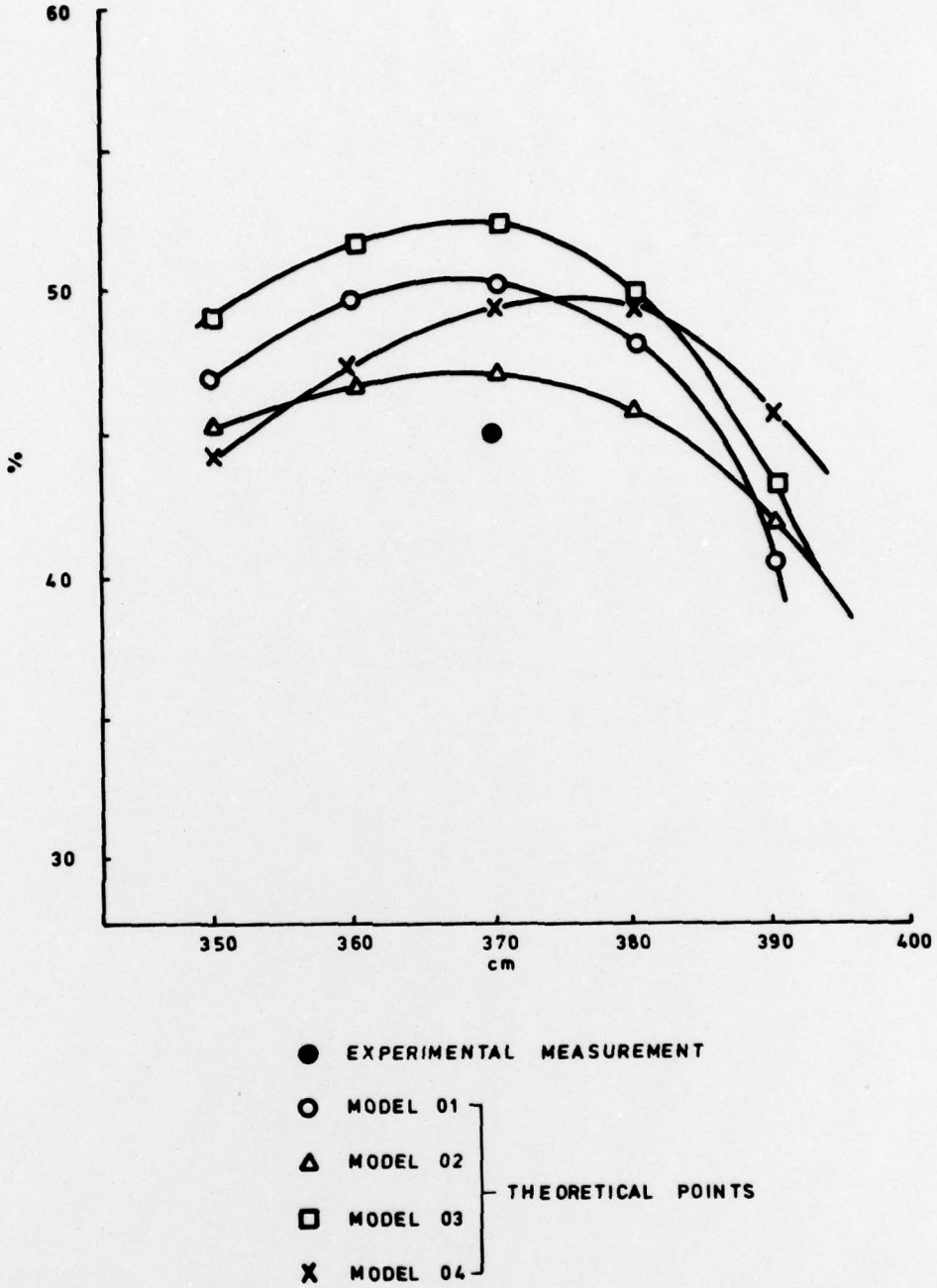

FIGURE 15 Fraction of Energy in Central Maximum versus Distance from 370 cm Focal Length Mirror

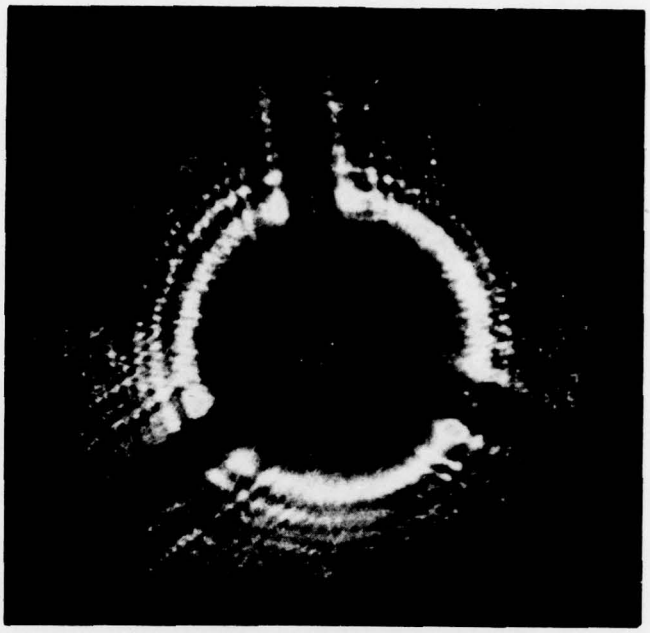

FIGURE 16. NEAR FIELD BURN PATTERN SHOWING THE FINE RING STRUCTURE AND THE EFFECT OF THE THREE-LEGGED MIRROR

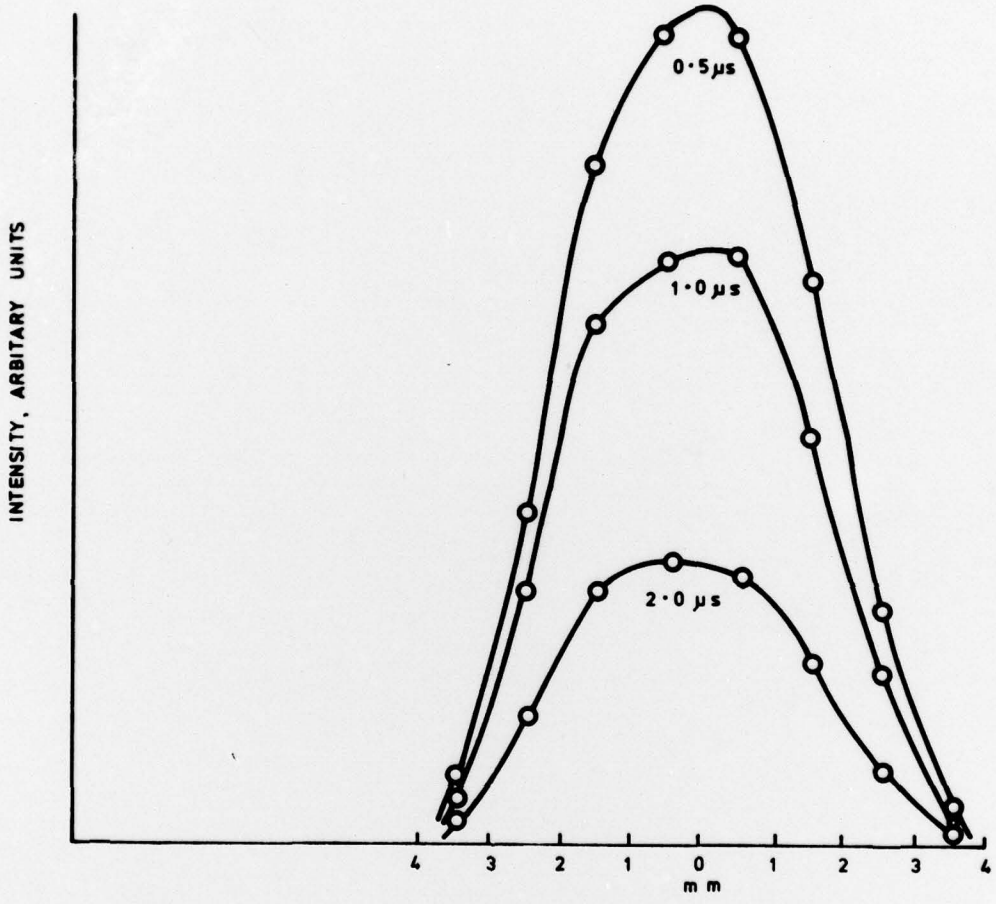

FIGURE 17 Focal Plane Profiles Recorded at 0·5, 1·0 and 2·0μs

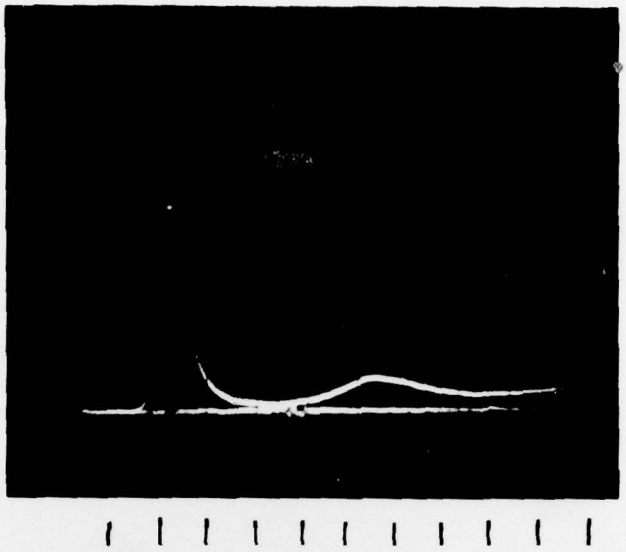

0.2 μs per division

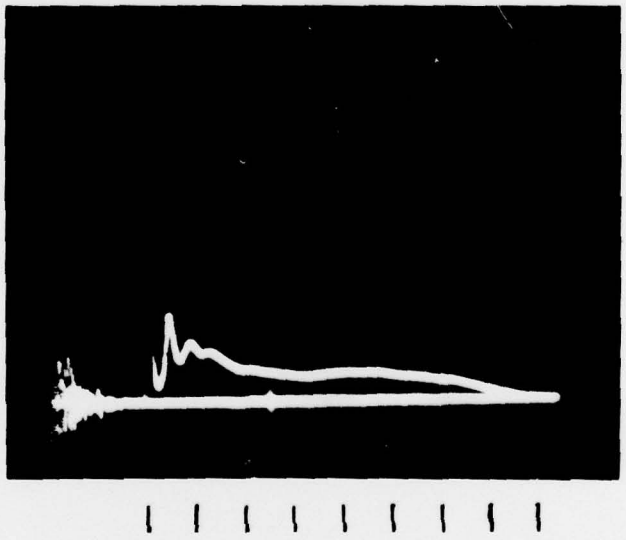

2 μs per division

FIGURE 18. TEMPORAL PROFILE OF TEAL USING A CO_2:CO:He GAS MIXTURE

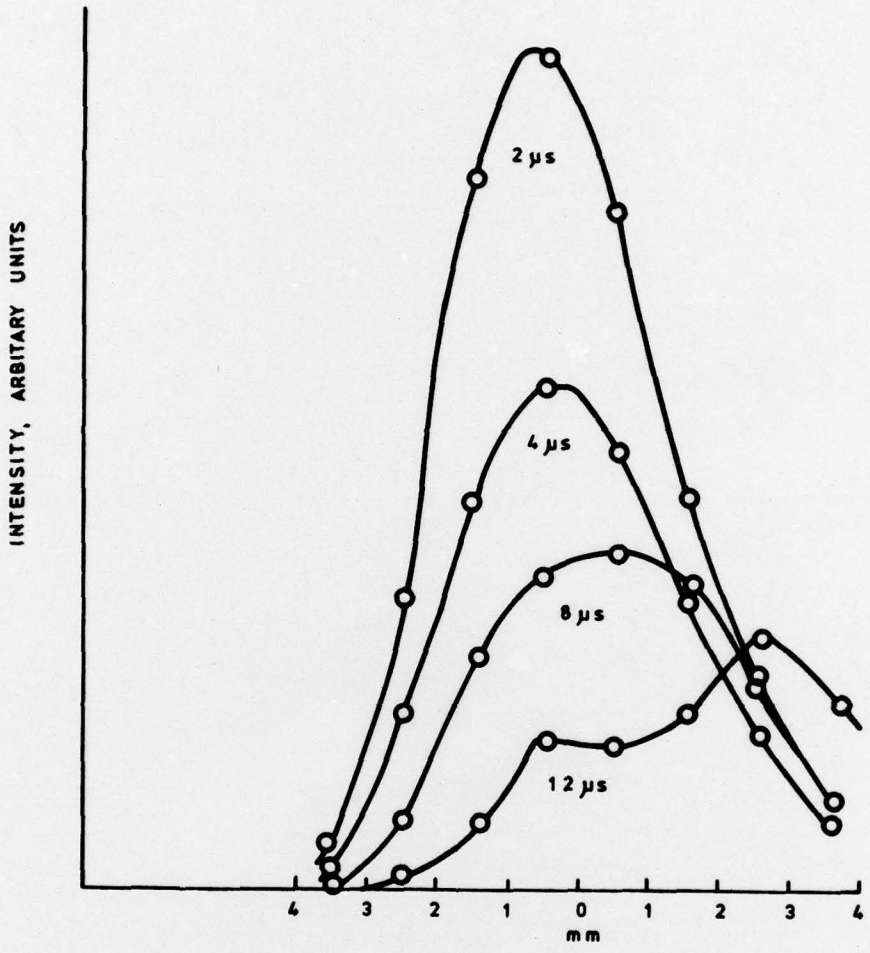

FIGURE 19 Spatial Profile in the Focal Plane as a Function of Time, using a CO_2 : CO : He Gas Mixture

DOCUMENT CONTROL SHEET

Overall security classification of sheet UNCLASSIFIED

(As far as possible this sheet should contain only unclassified information. If it is necessary to enter classified information, the box concerned must be marked to indicate the classification eg (R), (C) or (S)).

1. DRIC Reference (if known)	2. Originator's Reference	3. Agency Reference	4. Report Security Classification
----	AWRE Report No. 09/79	-	UNLIMITED

5. Originator's Code (if known)	6. Originator (Corporate Author) Name and Location
-	Atomic Weapons Research Establishment, Aldermaston, Berkshire

5a. Sponsoring Agency's Code (if known)	6a. Sponsoring Agency (Contract Authority) Name and Location
-	-

7. Title

The Construction and Performance of TEAL

7a. Title in Foreign Language (in the case of Translation)

-

7b. Presented at (for Conference Papers). Title, Place and Date of Conference

-

8. Author 1.Surname, Initials	9a. Author 2	9b. Authors 3, 4	10. Date	pp	ref
Eggins P L	Prosser R J	Simmons A C	June 1979	32	7

11. Contract Number	12. Period	13. Project	14. Other References
-	-	-	-

15. Distribution Statement

No restriction

16. Descriptors (or Keywords) (TEST)

Lasers
Carbon dioxide lasers

Abstract

The construction of TEAL (Transversely Excited Atmospheric pressure Laser) is described with reference to the required specification for single pulse thermal blooming experiments. All the major performance parameters are described, such as energy, temporal profile, spectrum and stability. In particular, several different measurements of the spatial profile are compared with theoretical predictions, which in general predict well the main features but not the finer details. Also the results of pulse stretching experiments are described, in which the pulse is lengthed from 3 to 14 μs.

micro sec

Some Metric and SI Unit Conversion Factors

(Based on DEF STAN 00-11/2 "Metric Units for Use by the Ministry of Defence", DS Met 5501 "AWRE Metric Guide" and other British Standards)

Quantity	Unit	Symbol	Conversion
Basic Units			
Length	metre	m	1 m = 3.2808 ft 1 ft = 0.3048 m
Mass	kilogram	kg	1 kg = 2.2046 lb 1 lb = 0.45359237 kg 1 ton = 1016.05 kg
Derived Units			
Force	newton	$N = kg\ m/s^2$	1 N = 0.2248 lbf 1 lbf = 4.44822 N
Work, Energy, Quantity of Heat	joule	J = N m	1 J = 0.737562 ft lbf 1 J = 9.47817×10^{-4} Btu 1 J = 2.38846×10^{-4} kcal 1 ft lbf = 1.35582 J 1 Btu = 1055.06 J 1 kcal = 4186.8 J
Power	watt	W = J/s	1 W = 0.238846 cal/s 1 cal/s = 4.1868 W
Electric Charge	coulomb	C = A s	-
Electric Potential	volt	V = W/A = J/C	-
Electrical Capacitance	farad	F = A s/V = C/V	-
Electric Resistance	ohm	Ω = V/A	-
Conductance	siemen	$S = 1\ \Omega^{-1}$	-
Magnetic Flux	weber	Wb = V s	-
Magnetic Flux Density	tesla	$T = Wb/m^2$	-
Inductance	henry	H = V s/A = Wb/A	-
Complex Derived Units			
Angular Velocity	radian per second	rad/s	1 rad/s = 0.159155 rev/s 1 rev/s = 6.28319 rad/s
Acceleration	metre per square second	m/s^2	$1\ m/s^2 = 3.28084\ ft/s^2$ $1\ ft/s^2 = 0.3048\ m/s^2$
Angular Acceleration	radian per square second	rad/s^2	-
Pressure	newton per square metre	N/m^2 = Pa	$1\ N/m^2 = 145.038 \times 10^{-6}\ lbf/in^2$ $1\ lbf/in^2 = 6.89476 \times 10^3\ N/m^2$
	bar	bar = $10^5\ N/m^2$	- 1 in. Hg = 3386.39 N/m^2
Torque	newton metre	N m	1 N m = 0.737562 lbf ft 1 lbf ft = 1.35582 N m
Surface Tension	newton per metre	N/m	1 N/m = 0.0685 lbf/ft 1 lbf/ft = 14.5939 N/m
Dynamic Viscosity	newton second per square metre	$N\ s/m^2$	$1\ N\ s/m^2 = 0.0208854\ lbf\ s/ft^2$ $1\ lbf\ s/ft^2 = 47.8803\ N\ s/m^2$
Kinematic Viscosity	square metre per second	m^2/s	$1\ m^2/s = 10.7639\ ft^2/s$ $1\ ft^2/s = 0.0929\ m^2/s$
Thermal Conductivity	watt per metre kelvin	W/m K	-
Odd Units*			
Radioactivity	becquerel	Bq	1 Bq = 2.7027×10^{-11} Ci 1 Ci = 3.700×10^{10} Bq
Absorbed Dose	gray	Gy	1 Gy = 100 rad 1 rad = 0.01 Gy
Dose Equivalent	sievert	Sv	1 Sv = 100 rem 1 rem = 0.01 Sv
Exposure	coulomb per kilogram	/kg	1 C/kg = 3876 R 1 R = 2.58×10^{-4} C/kg
Rate of Leak (Vacuum Systems)	millibar litre per second	mb l/s	1 mb = 0.750062 torr 1 torr = 1.33322 mb

*These terms are recognised terms within the metric system.